

Proton capture on ^{34}S in the astrophysical energy regime of O-Ne novae

M. Lovely,¹ A. Lennarz,² D. Connolly,^{2,3} M. Williams,^{2,4} M. Alcorta,² A. A. Chen,⁵ B. Davids,² N. E. Esker,² C. Fry,⁶ S. A. Gillespie,² R. Giri,⁷ U. Greife^{⊗,1,*}, A. Hussein,⁸ D. Hutcheon,² J. Karpesky,¹ L. Kroll,⁵ J. Liang,⁵ P. D. O'Malley,⁹ S. Paneru,⁷ A. Psaltis,⁵ C. Ruiz,² and A. C. Shotton¹⁰
(DRAGON Collaboration)

¹Colorado School of Mines, Golden, Colorado 80401, USA

²TRIUMF, Vancouver, British Columbia V6T 2A3, Canada

³Los Alamos National Laboratory, Los Alamos, New Mexico 87545, USA

⁴University of York, York YO10 5DD, United Kingdom

⁵McMaster University, Hamilton, Ontario L8S 4L8, Canada

⁶Michigan State University, East Lansing, Michigan 48824, USA

⁷Ohio University, Athens, Ohio 45701, USA

⁸University of Northern British Columbia, Prince George, British Columbia V2N 4Z9, Canada

⁹University of Notre Dame, Notre Dame, Indiana 46556, USA

¹⁰University of Edinburgh, Edinburgh EH9 3FD, United Kingdom



(Received 7 December 2020; accepted 13 April 2021; published 6 May 2021)

Nuclear reaction sensitivity studies have shown that the final isotopic abundance of O-Ne nova nucleosynthesis is dependent on the $^{34}\text{S}(p, \gamma)^{35}\text{Cl}$ reaction at astrophysical energies corresponding to peak nova burning temperatures of 0.1–0.4 GK. Isotopic ratios of the S, Cl, and Ar products are all used in various methods of cosmochemical analysis of presolar meteoritic grains. Due to the lack of direct experimental data, the $^{34}\text{S} + p$ reaction rate has been estimated using statistical modeling or information from indirect nucleon transfer experiments. In order to provide direct reaction information, the resonance strengths of several low energy resonances, $E_{\text{c.m.}} = 272\text{--}495$ keV, in the $^{34}\text{S}(p, \gamma)^{35}\text{Cl}$ reaction were measured for the first time in inverse kinematics using the DRAGON recoil separator located at TRIUMF, Canada's Particle Accelerator Centre in Vancouver.

DOI: [10.1103/PhysRevC.103.055801](https://doi.org/10.1103/PhysRevC.103.055801)

I. INTRODUCTION

Explosive nucleosynthesis, such as in classical novae, proceeds mainly via successive proton capture on stable and radioactive nuclides. Due to the high densities and temperatures at which these processes occur, the proton capture reaction rates can exceed the competing β^+ decay, which therefore drives nucleosynthesis to higher masses on the proton rich side of the valley of stability [1]. Novae occur due to the thermonuclear runaway of accreted material onto the surface of a white dwarf in a binary system with a main sequence star. The hydrogen rich materials from the main sequence companion fuel the pp (proton-proton) chain and eventually the hot CNO (carbon-nitrogen-oxygen) cycle after mixing with the outer layers of the white dwarf (for more detailed information see [2–4]). This leads to thermonuclear runaway until an explosion takes place in which, on average, $2 \times 10^{-5} M_{\odot}$ of material can be ejected into the interstellar medium [2]. The ejected material provides a source of galactic isotopic enrichment and can leave a unique signature in the presolar meteoritic grains that may eventually form. These

explosions do not destroy the progenitor system and can recur over relatively short periods of time [5]. O-Ne (oxygen-neon) novae make up 33% of the observed novae with an estimated rate of 25 to 80 novae occurring galactically per year [6]. As a result of their unique conditions, novae are the main source of isotopes like ^{17}O , ^{15}N , and ^{13}C [7].

Presolar meteoritic grains are small (of order μm) grains that condensed prior to the formation of the solar system. These then became embedded within other material and formed meteorites of which some subsequently impacted the Earth. By analyzing the unique chemical composition of these grains, the potential production site type can be determined. These grains constitute the only means of obtaining and analyzing nova material directly. One method of determining the source is the comparison of the isotopic ratios of various elements to the ratios seen in solar abundances. Due to the unique environments in explosive nucleosynthesis, isotopic production ratios can vary drastically. For example, the radioactive isotope ^{22}Na , which is produced in novae, eventually decays into ^{22}Ne *in situ* and therefore leaves an increased $^{22}\text{Ne} / ^{20}\text{Ne}$ ratio compared to the solar ratio [8]. It has been shown that novae and supernovae can produce low $^{12}\text{C} / ^{13}\text{C}$ and $^{14}\text{N} / ^{15}\text{N}$ ratios that currently cannot be explained by other sources [9]. For grains produced in novae, the ratios of

*ugreife@mines.edu

$^{26}\text{Al}/^{27}\text{Al}$ and $^{30}\text{Si}/^{28}\text{Si}$ are expected to be large relative to solar values [10,11]. More recently, it has been shown that use of $^{33}\text{S}/^{32}\text{S}$ and $^{34}\text{S}/^{32}\text{S}$ ratios may also provide the ability to distinguish novae grains from those of supernovae sources [12–14].

The radiative proton capture of ^{34}S in nova environments, which produces ^{35}Cl , has been shown to be sensitive to the strength of resonant states at energies corresponding to the peak burning temperature 0.1–0.4 GK (Gamow peak range for this reaction is within $E_{c.m.} \approx 120\text{--}550$ keV). The astrophysical reaction rates in this energy regime have been estimated using statistical model calculations. Varying these rates within the estimated uncertainties of the statistical model approach of up to a factor 100 up or down leads in some O-Ne nova models to variation in the expected production of ^{35}Cl and ^{36}Ar by factors of 20 and 7, respectively [3,15]. The exploration of the relevant energy range for the existence of resonant states and direct measurement of their strengths, where possible, is needed in order to reduce the uncertainty in the production of these nuclides.

II. PREVIOUS WORK ON $^{34}\text{S}(p, \gamma)^{35}\text{Cl}$ RESONANCES

The $^{34}\text{S}(p, \gamma)^{35}\text{Cl}$ reaction (Q value = 6370.8 keV) had been directly studied at proton energies down to 388 keV [16]. However, this previous experiment did not have the sensitivity to detect resonant features below the resonance at $E_{c.m.} = 495$ keV. All previous studies [16–20] utilized forward kinematics with proton beams and solid targets of sulfur compounds. Due to the target stoichiometries and enrichment levels being possible sources of error, as well as proton beam induced γ -ray backgrounds in the detectors, the experiments could be susceptible to unrecognized systematic errors. Their resonant yields were typically measured relative to a previously measured, and presumed to be well known, resonance strength. In this reaction the characteristic reference state mostly used was the $E_{c.m.} = 1177$ keV resonance. It was originally measured in 1963 [17] to have a strength of 2.0(6) eV; however, probed again in 1966, it was assigned a resonance strength of 10.5(15) eV [18]. Another experiment in 1974 reported a resonance strength of 4.9(5) eV [19]. Depending on the value used, the resulting strengths in any relative measurement vary by a factor of over 5. The 495 keV resonance strength value, to which we compare our measurement, was determined relative to the 695 keV state in [16], which itself was measured relative to the 1177 keV state in [20] using the reference resonance strength from [18]. Other studies that attempted to reach lower in energy relied on indirect methods populating excited states in ^{35}Cl through ($^3\text{He}, d$) and (α, p) transfer reactions [14,21–23]. Several recent indirect measurements have found new potential resonant states, many of which could have a significant impact on the astrophysical reaction rate. Specifically, in the ($^3\text{He}, d$) measurement by Gillespie *et al.* [14], ten new potential resonant states were determined below the previously confirmed resonance at $E_{c.m.} = 495$ keV. Not all of the new resonances are predicted to have significant strength. However, the states corresponding to potential resonances at center of mass energies of 272 keV and 303 keV have the potential to dominate the production of

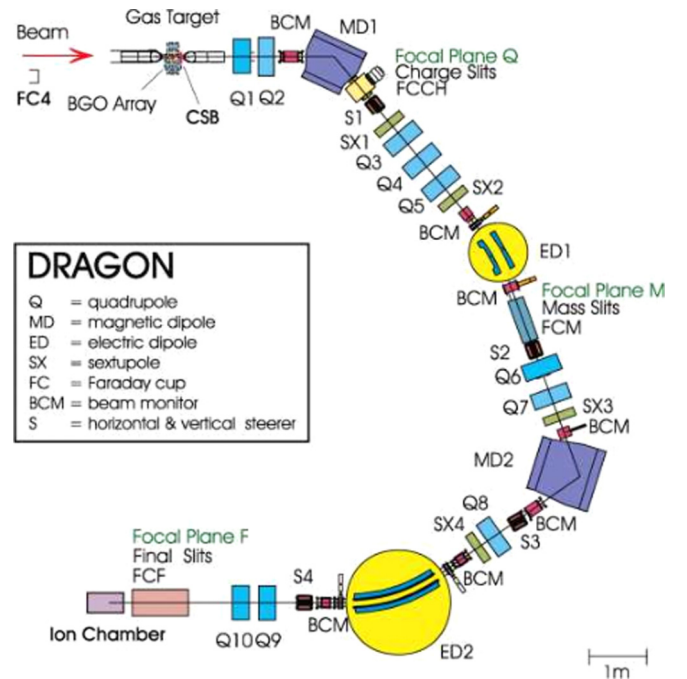


FIG. 1. Schematic of the DRAGON recoil separator showing the magnetic dipoles (MD) and electric dipoles (ED) as well as other separator elements necessary for ion transport and analysis.

^{35}Cl in nova environments. A follow-up measurement at the Triangle Universities Nuclear Laboratory (TUNL; published after the experiment presented here was performed), which utilized the (α, p) transfer, did observe the 303 keV but not the 272 keV state [21].

III. EXPERIMENTAL SETUP

The current work was performed in inverse kinematics, which utilizes a heavy ion beam of ^{34}S , produced by the off line ion source (OLIS) in the isotope separator and accelerator (ISAC) experimental hall located at TRIUMF, Canada's Particle Accelerator Centre in Vancouver, Canada. Due to the charge-to-mass acceptance of the ISAC accelerator ($3 \leq A/q \leq 6$) the beam was provided in the 7^+ charge state at intensities of order $10^{10}\text{--}10^{11}$ ions/s [24,25]. Once accelerated to the required energies, the beam was delivered to the detector of recoils and gammas of nuclear reactions (DRAGON).

DRAGON is a 21 m long, two stage electromagnetic separator which is primarily used to measure resonance strengths in proton or α radiative capture reactions with stable or radioactive ion beams at energies relevant to explosive nucleosynthesis [26–28]. DRAGON has four main components (see Fig. 1): the differentially pumped windowless gas target, a high efficiency γ -detecting BGO (bismuth germanate) array, the two stage electromagnetic separator, and heavy ion detector systems near the final focal plane.

The windowless gas target can maintain pressures of 2–10 Torr of hydrogen or helium gas within an effective length of 12.3(4) cm [29]. The target gas streaming through its gas flow limiting apertures (their diameter matched to the angular acceptance of the recoil separator) is pumped through a series

of turbomolecular and roots blower pumps and is filtered through an LN_2 cooled zeolite trap to remove impurities. The controlled recirculation of gas as well as small target entrance and exit apertures maintain the gas pressure within 5% throughout the course of an experiment. The vacuum upstream and downstream of the target is maintained by a series of differential pumping stages at a level of $\leq 3 \times 10^{-6}$ Torr [30]. Inside of the target are two silicon surface barrier detectors positioned at well-collimated angles of 30° and 57° relative to the beam path. These are used to detect the rate of elastically scattered protons or α particles, which is directly proportional to the incoming beam intensity and the gas pressure. The latter is measured by a capacitance manometer and is kept constant to within a few percent. Any fluctuations in beam current that occur during the run can be accounted for by normalizing the rate of scattered protons or α s to absolute current measurements using Faraday cups inserted into the beam path for short time periods before and after each run [1].

DRAGON's γ -photon detecting BGO array is composed of 30 closely packed hexagonal crystals which provide a solid angle coverage of $\approx 90\%$ from the center of the target [31,32]. The BGO array is used to detect the promptly emitted γ photons from the de-excitation of the compound recoil nuclei as a method of coincidence tagging of the heavy ion recoils arriving in the separator focal plane. Photon detection time is used in conjunction with the heavy ion focal plane arrival time to create a separator time of flight (TOF) parameter for particle identification (PID). The γ -photon detection can also be used to calculate the position of the resonance within the target by correlating the distribution of the registered γ photons over the individual crystals of the array [33].

The major component of DRAGON is the electromagnetic separator composed of two stages, each with one magnetic and one electrostatic dipole. The first magnetic dipole is used to select the desired charge state (of a fixed momentum) since the beam will undergo a series of charge-exchange reactions in the target gas which leave the beam and recoils in an equilibrium distribution of charge states upon exiting the target. Only one charge state can be transported through the length of DRAGON and typically the most populated charge state is chosen to maximize the number of detected recoils. Any beam or recoil particles not in the chosen charge state hit a first set of current reading slits located downstream of the magnetic dipole. As beam and recoils carry essentially the same momentum and the charge has been selected, the transported mass can be chosen by using the electrostatic dipoles as a kinetic energy filter. Since the recoil nuclei have picked up an additional nucleon in the case of (p, γ) reactions, they are separated from the beam particles at the first energy-focused (mass-dispersed) focal plane with another set of current reading slits located downstream of the first electrostatic dipole. This process is then repeated with a second set of magnetic and electrostatic dipoles to allow DRAGON to achieve of order 10^9 - 10^{13} direct beam suppression depending on energy and recoil/beam combination [34].

The final section of DRAGON is comprised of a series of heavy ion detectors determining the velocity and kinetic energy of the ions that reach the focal plane. The velocity measurement consists of two microchannel plate (MCP) detectors

which use secondary electrons from the interaction of the ions with thin carbon foils intercepting the beam path. The two detectors are separated by 57 cm which allows them to produce a local TOF parameter [28]. For the energy measurement, following the MCP detectors, interchangeably, either a double sided silicon strip detector (DSSSD), an ionization chamber (IC), or a hybrid detector, which utilizes both a DSSSD and IC, can be installed. For the present work the hybrid detector was used as it was expected to provide some means of PID which, however, as the experiment was performed, turned out to be not sufficient to rely only on focal plane detectors for recoil identification. Therefore, this analysis had to use coincidence conditions between the BGO array and focal plane detectors to achieve a clean reaction recoil detection.

IV. EXPERIMENTAL APPROACH

In inverse kinematic experiments, the quantity measured is the number of recoil nuclei detected and identified at the focal plane. This quantity is then related to the total number of reactions by factoring in the various transmission probabilities and detection efficiencies of all components of DRAGON. The total efficiency for this experiment is given by

$$\eta_{\text{tot}} = \eta_{\text{BGO}} \eta_{\text{CSF}} \eta_{\text{sep}} \eta_{\text{MCP}}^{\text{trans}} \eta_{\text{live}} \eta_{\text{Hy}}, \quad (1)$$

where η_{BGO} is the BGO detection efficiency, η_{CSF} is the fraction of recoils in the selected charge state, η_{sep} is the recoil transmission through the separator stages of DRAGON, $\eta_{\text{MCP}}^{\text{trans}}$ is the transmission through both MCP assemblies (carbon foils and wire mesh for electron deflection), η_{live} is the electronics' live time, and η_{Hy} is the hybrid detector efficiency.

To determine the BGO efficiency several GEANT3 simulations were performed for each individual resonance [31,35]. The total BGO detection efficiency depends on the multiplicity, energy, and emission pattern of the γ rays emitted. Since branching ratio and decay scheme information only existed for the ^{35}Cl excited state which correlates to the 495 keV resonance [16], an upper and lower limit efficiency simulation was undertaken for each state. The lower limit assumed a direct to ground state transmission (100%) and the upper limit simulation assumed a 3- γ cascade through known states allowed by spin-parity selection rules (100%). The number of possible combinations was limited (due to the need to reduce the phase space that needed to be explored) by the requirement that the photon energy was greater than 1.5 MeV (lower energy photons would lower the efficiency due to the individual detector cutoffs used). For the same reason, only isotropic emission patterns were simulated. The simulation of the 495 keV resonance used the existing γ -decay scheme information [16], which, however, was also compared to the upper and lower limit simulations. The result based on the known gamma emission agreed well with the average of the two simulations. For all other resonances the average was used for the BGO efficiencies, see Table I for a list of the applied efficiencies. The error (which is one of the major error components) was chosen to include both upper and lower limits relating to the branching ratio issues discussed above and is given in this paper in parenthesis (to be applied as a \pm interval on the last digits of the given values).

TABLE I. BGO simulation results for energies probed in this experiment; potential resonance energies and uncertainties from Gillespie *et al.* [14] and Endt [36].

$E_{c.m.}$ [keV]	Simulated BGO efficiencies		
	$\eta_{BGO,up}$ [%]	$\eta_{BGO,low}$ [%]	η_{BGO} [%]
495.5(6)	88.1	61.6	73.6(74)
471(2)	88.3	61.9	75.0(132)
452(2)	88.1	62.3	75.0(129)
431(4)	88.6	61.5	75.0(136)
407(2)	88.2	61.0	75.0(136)
390(2)	88.6	63.2	76.0(127)
303(2)	87.3	62.3	75.0(125)
272(2)	88.0	62.0	75.0(130)

The fraction of recoils in a particular charge state was measured directly at DRAGON using a beam of the recoil ion, in this case ^{35}Cl , accelerated to the same velocity range as the recoils produced during the proton capture experiment. By comparing the beam current before charge selection to the Faraday cup downstream of the first dipole magnet and its associated set of slits, the charge state fraction is determined for a specific energy $E_{out,rec,lab}$ of the recoils when exiting the gas target (measured with the first magnetic dipole MD1 of DRAGON). This is repeated for all charge states that can be bent by the first magnetic dipole and typically a full distribution can be inferred from the main charge state distribution (CSD) components measured. The measured CSDs are fit with a Gaussian distribution to determine the mean and width. It has been seen that the width is roughly constant for any given ion type and the mean varies linearly with energy [37,38]. The fit parameters, mean and width of the CSDs, can be used to interpolate the values at the desired energy (Fig. 2 shows a comparison of the CSDs measured in this work with the prediction based on a semi-empirical formula

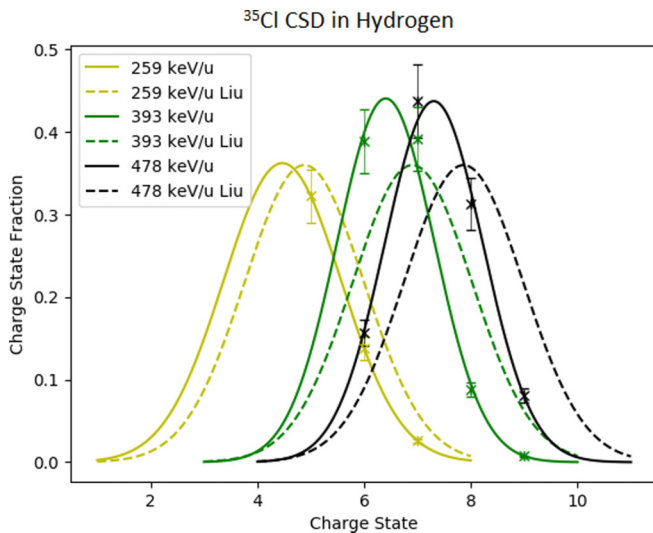


FIG. 2. ^{35}Cl equilibrium CSD measurements from this work compared to the prediction by Liu *et al.* [38] (noted is the beam energy after traversing the target filled with 5–6 Torr hydrogen gas).

TABLE II. Charge state fractions (CSF) used for recoil calculations.

$E_{c.m.}$ [keV]	$E_{out,rec,lab}$ [keV/u]	q^+	CSF [%]
495.5(6)	471.4(5)	8	30.7(17)
471(2)	444.2(5)	8	22.3(22)
452(2)	425.9(5)	8	16.9(27)
431(4)	407.7(5)	8	12.3(34)
407(2)	385.8(5)	6	41.0(16)
390(2)	368.4(5)	6	42.9(40)
303(2)	284.0(5)	5	42.4(47)
272(2)	255.3(5)	5	42.7(42)

from Liu *et al.* [38] using data from experiments with lighter ions). Using a Gaussian with the interpolated mean and width and normalizing to unity, the charge state fraction for any given charge state (q^+) of the recoil ions was determined. See Table II for a list of the resulting charge state fractions.

After radiative capture of the beam nucleus, the compound reaction products (recoil nuclei) are typically in an excited state and emit one or more photons. This imparts a small amount of momentum that will vary the trajectory of the recoils depending on their mass and the energy of the γ photons. As a result the recoils exit the target into a cone of a maximum half angle which correlates to a single γ ray being emitted perpendicular to the beam axis, described by the equation [3]

$$\phi_{max} = \tan^{-1}\left(\frac{E_{\gamma}}{\sqrt{2m_b c^2 E_b}}\right), \quad (2)$$

where E_{γ} is the maximum γ energy, E_b and m_b are the beam energy and mass, and c is the speed of light. DRAGON has a nominal angular acceptance of ± 21 mrad and in this experiment the largest ϕ_{max} that could have occurred results in ± 8.6 mrad, fitting thus comfortably into the acceptance cone. Therefore, the canonical value of the DRAGON separator transmission, 99.9(1)% was used [27].

In order to determine the transmission through the MCP carbon foils and electron mirror grids, data were taken with attenuated (in order to protect the focal plane detectors from heavy ion induced damage) ion beam steered to the hybrid detector with and without the MCP assemblies in place. For this experiment, the MCP transmission was determined to be 76.6(9)%, which agrees well with the previous measurement of the MCP transmission of 76.9(6)% [30]. The livetime efficiency η_{live} (Table III) is determined through an analysis of the data acquisition (DAQ) busy times at both the BGO and focal plane systems.

The final efficiency factor needed is the hybrid efficiency η_{Hy} (Table III). The hybrid efficiency is determined primarily by the DSSSD efficiency as the IC stage has by design approximately full detection efficiency for ions passing at shallow angles into the detector. The hybrid detection efficiency can be found using the equation

$$\eta_{Hy} = \frac{N_{DSSSD}}{N_{IC}}, \quad (3)$$

where N_{DSSSD} and N_{IC} are the number of counts in the full energy peak of the DSSSD and IC, respectively. This was

TABLE III. Target transmission, electronics live time, and hybrid detector efficiency.

$E_{c.m.}$ [keV]	τ_{tgt}	$\eta_{live,c}$	η_{Hy}
495.5(6)	0.940(18)	0.745(7)	0.900(7)
471(2)	0.926(17)	0.740(23)	0.882(55)
452(2)	0.950(12)	0.735(10)	0.946(44)
431(4)	0.943(21)	0.757(14)	0.833(70)
407(2)	0.927(13)	0.827(4)	0.949(44)
390(2)	0.907(19)	0.746(5)	0.897(22)
303(2)	0.921(14)	0.735(11)	0.904(10)
272(2)	0.914(3)	0.745(7)	0.890(6)

determined to be 89.7(4)% on average for this work, but specific values (Table III) were applied for each resonance.

In addition, the total number of incoming beam particles needs to be calculated. The yield measurement at each resonance energy is comprised of several 1-h runs. At the beginning and end of each run the beam intensity is determined using a series of Faraday cups located up- and downstream of the target. To account for any fluctuations in beam intensity that occur during the course of these runs, a beam normalization coefficient, R , that correlates the data from the elastic scattering monitors to the absolute Faraday cup readings, is calculated as

$$R = \frac{I}{qe} \frac{\Delta t}{N_p} \tau_{tgt}. \quad (4)$$

Here, I is the average current measured in the Faraday cup upstream of the target, q is the beam charge, e is the elementary charge, N_p is the number of scattered protons in the silicon surface barrier detector's full energy peak during the time Δt , and τ_{tgt} is the transmission through the gas target (Table III, using Faraday cup readings directly up- and downstream of the target without gas). An average normalization coefficient for a given beam energy, \bar{R} , is calculated and then used to determine the number of incoming beam particles for each individual run as

$$N_b = \bar{R} N_{p,tot}, \quad (5)$$

where $N_{p,tot}$ is the total number of scattered protons during the entire run and N_b is the number of beam particles for the given run.

Once the number of reactions that occurred (N_{rxn}) has been determined using the number of recoils detected divided by the total efficiency η_{tot} , the thick target yield, Y_∞ , can be calculated

$$Y_\infty = \frac{N_{rxn}}{N_b}. \quad (6)$$

The resonance strength is then

$$\omega\gamma = 2 \frac{Y_\infty}{\lambda_r^2} \epsilon_r \frac{m_t}{m_b + m_t}, \quad (7)$$

where m_t is the target mass, ϵ_r is the laboratory frame stopping power, and λ_r is the center of mass de Broglie wavelength. The laboratory frame stopping power is determined by measurements of the beam energy with and without gas in the

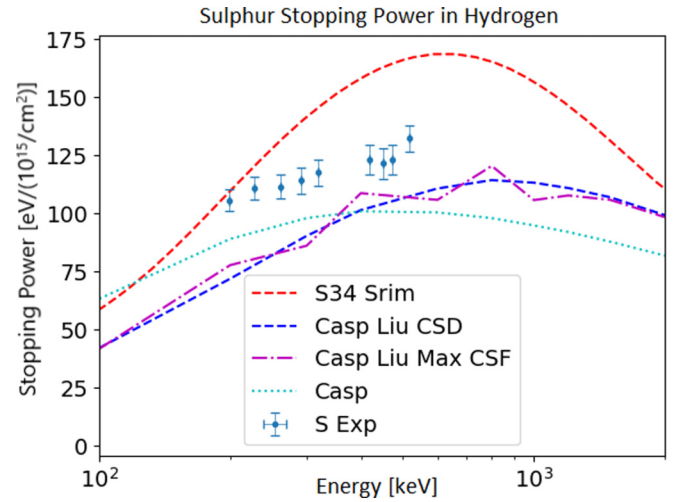


FIG. 3. Stopping power data measured in this experiment compared to the available codes SRIM [39] and CASP [40]. In the case of CASP, which provides charge state dependent stopping power information, several assumptions on charge state distributions were tried, however, as with SRIM, no satisfactory predictive description can be achieved (for details see [41]).

target using the first magnetic dipole to center the beam on the first set of current reading slits. Using the required magnetic field to center the beam on the slits and the equation

$$E_{lab} = c_{mag} \left(\frac{qB}{m_b} \right)^2, \quad (8)$$

the kinetic energy is calculated. Here, c_{mag} is the magnetic constant of the dipole, 0.0004815 keV/amu/G² (determined through an experimental campaign using well-known resonances [27]), q is the charge state, and B is the magnetic field strength (in Gauss) required to center the beam. The stopping power is expressed as

$$S(E) = \frac{\Delta E}{\Delta A} m_b 10^{18}, \quad (9)$$

where $S(E)$ is the stopping power in units of $\frac{\text{eV}}{(10^{15}/\text{cm}^2)}$, ΔA is the change in areal target density (gas in - gas out), and m_b is expressed in units of amu. A (in units of $1/\text{cm}^2$) can be found using

$$A = 9.66 \times 10^{18} \nu \frac{P}{Tl}, \quad (10)$$

where ν is the gas type, two for diatomic, T is the temperature in Kelvin, P is the pressure in Torr, and l is the effective target length in cm (from [4]). The stopping power data from this experiment are depicted in Fig. 3 compared to various approaches using semiempirical calculation from the two stopping power codes stopping range of ions in matter (SRIM) [39] and convolution approximation for swift particles (CASP) [40]. It is apparent that it is advantageous to perform a direct measurement of stopping power as the predictive capabilities of the current codes are limited.

In many DRAGON experiments at low beam energies, the local TOF using the MCP detectors had been used as the

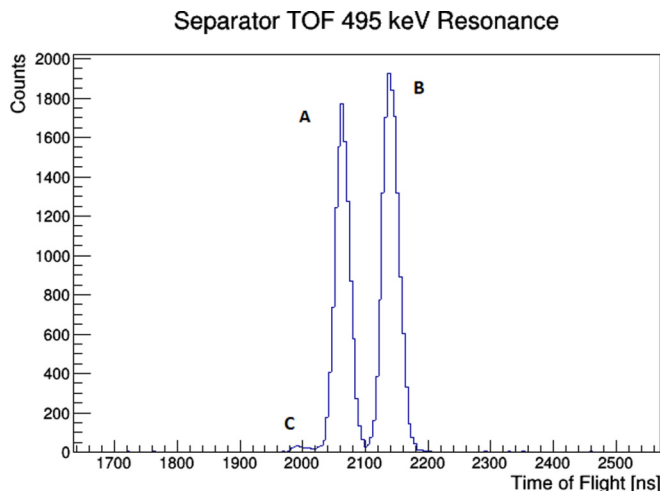


FIG. 4. Separator TOF for the 495 keV resonance. The two dominant timing peaks correspond to BGO start followed by MCP0 plus MCP1 recoil signals (A), and only a recoil signal in the hybrid (B). The weak peak (C) on the left is caused by a stop from an MCP0 recoil signal coinciding with random MCP1 noise.

primary means of PID in an attempt to allow for an analysis of just the reaction recoils without requiring detection of reaction photons. However, during the work presented here, the MCP detectors were experiencing a detrimental amount of electronic noise of unknown origin that caused the detection efficiency of the MCP assemblies to drastically decrease and vary with time. Therefore, the global TOF or separator TOF (which in contrast to the local TOF requires a start signal from the BGO array for coincidence analysis) was used as the primary tool to separate recoils from leaky beam signals. The arrival signal at the focal plane is triggered by the first focal plane detector system to produce a valid signal. With lower MCP efficiencies, this could be either a logic signal indicating both MCPs were triggered or by a hit in the hybrid detector. The separator TOF spectrum (Fig. 4) for our resonance with the highest yield (495.5 keV) shows several closely spaced peaks. All TOF intervals are started by the BGO array. The two dominant peaks show the stop signals as anticipated from either the hybrid detector or from a logic signal generated when both MCPs (as intended for the Local TOF) register a signal. However, due to the increased electronic noise mentioned above, these are preceded by a much weaker peak which likely contains events where a recoil ion triggered the first MCP while the required signal in the second MCP originates from a random noise signal. All signals are valid as this analysis also requires an event in the final hybrid detector. In order to encompass all events, the timing cut used in the separator TOF analysis needed to be increased to a time interval of 200 ns (while an individual detector peak spanned approximately 60 ns) and thereby decreased the sensitivity of the measurement (specifically in the determination of upper limits) due to the increased number of background counts to be taken into account. The interval width established at the $E_{c.m.} = 495$ keV resonance was also applied to the separator TOF data at the other energies through scaling to the expected

time of flight. It can also be seen that there is a small but roughly constant background outside of the signal region. These events are due to accidental coincidences between the room background photons and leaky beam reaching the end detectors. Since the events are uncorrelated, they occur at random times and produce a constant background that can be subtracted.

V. ANALYSIS AND RESULTS

A. Direct measurement of the 495 keV resonance

In this experiment the strength of the 495 keV resonance was directly measured for the first time without the need for normalization to a higher energy resonance. This was achieved using an incoming beam of approximately 10^{10} s^{-1} ^{34}S ions at a laboratory energy of 518.6 keV/u with a gas target pressure of 5.76(14) Torr H_2 . The outgoing beam energy was measured to be 499.6 keV/u, which meant the $E_{\text{lab}} = 505.7$ keV/u resonance was placed slightly downstream of the center of the target, but well contained within its effective length. Using Eq. (9), the stopping power was determined to be $128.8(137) \frac{\text{eV}}{(10^{15}/\text{cm}^2)}$ which significantly (29%) deviates from the value predicted by the SRIM code of $166.2 \frac{\text{eV}}{(10^{15}/\text{cm}^2)}$. Differences of this order of magnitude have been observed previously in inverse kinematics experiments of heavy ions on light gas targets where the semiempirical SRIM code has few data sets to draw information from as a basis of its prediction [29]. The outgoing recoils were chosen to be in the 8^+ charge state which was measured in a later beam time with a chlorine beam to contain 30.7(17)% of the total number of ions.

In Fig. 4 the global or separator TOF spectrum is depicted for the 495 keV state. There are two dominant peaks which are the result of the specific focal plane detector conditions as discussed earlier.

A total run time of ≈ 12 h at the 495 keV resonance resulted in the detection of 22946(152) recoil events. Based on the beam normalization coefficient at this energy, $6.47(12) \times 10^{15}$ ^{34}S ions impinged on the target. The recoil/ion separation achieved by combining online and offline analysis, corresponds to a beam suppression factor of about 10^{-12} . Using the efficiencies and transmission data introduced above as well as Eq. (7), the resonance strength was calculated to be $1.37(22) \times 10^{-2}$ eV. The most recent relative measurement done by Prussien *et al.* [16] yielded a resonance strength of $2.5(13) \times 10^{-2}$ eV and used the largest value for the 1177 keV state of 10.5(15) eV measured by [18] as a reference. Despite the large error of the Prussien measurement, it is only barely in agreement. However, there is a strong likelihood that the value used for reference is in error and the factor 2 lower reference value of 4.9(5) eV determined for the 1177 keV resonance in a different experiment would be more accurate [19].

B. Direct measurement of the 272 keV resonance

The 272 keV resonance had never been directly measured, but has only been seen as a potential resonant state in the recent work by Gillespie *et al.* [14]. The strength inferred from the transfer reaction experiment was given as 8.6–8.9 \times

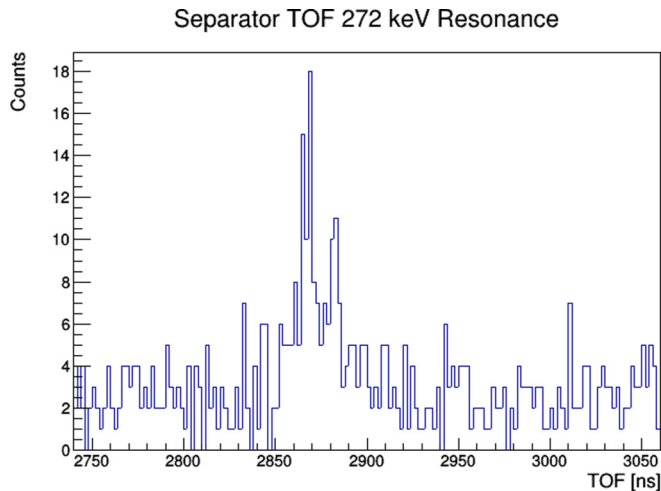


FIG. 5. Separator TOF for the 272 keV resonance. Again a 200 ns wide TOF gate was applied around the visible peak region to account for the detector issues encountered.

10^{-6} eV. With a resonance strength within this range, this resonance would dominate the astrophysical reaction rate at peak nova burning temperatures of 0.1–0.4 GK. In the present work, ^{34}S beam was provided at an energy of 287.3 keV/u and the target pressure averaged at 5.96(2) Torr. The outgoing beam energy was measured at the first magnetic dipole to be 271.7 keV/u. This means the $E_{\text{lab}} = 277.9$ keV/u resonance was again well contained within and just slightly downstream of the center of the gas target. The 5^+ recoil charge state was chosen as it was expected to populate the largest charge state fraction, later confirmed as 42.7(42)%. With low statistics and changed electronics settings on the MCPs, which reduced their noise but also their sensitivity, here only one recoil peak is clearly visible in the separator TOF, Fig. 5. Nevertheless, in order to account for the electronics issues, still a 200 ns wide TOF gate was applied around the peak region. Compared to the measurement at 495 keV, the occurrence of random events in the spectrum is increased due to larger number of integrated incident beam but also due to lower incident beam suppression by the DRAGON separator elements at lower beam energies [34]. Background subtraction resulted in the detection of a total of 101(19) recoil events over the approximately 40 h of experimental time with the total beam on target integrated to $1.02(8) \times 10^{16}$ ions. Performing the same analysis as for the 495 keV resonance results in a resonance strength of $1.22(36) \times 10^{-5}$ eV, $\approx 40\%$ above the value inferred by Gillespie *et al.* [14] from a transfer reaction measurement. The direct DRAGON experiment confirms the dominant nature of this resonance in the nova astrophysical regime for this reaction.

C. Further resonance strengths and upper limits

While the experiment was laid out to focus on the previously known 495 keV resonance as well as the potential astrophysically relevant resonance at 272 keV, other states in between that could possibly produce a measurable yield were also probed. In the available beam time, the runs at other

TABLE IV. Summary of resonance strengths and upper limits (all 1σ confidence level) of this experiment compared to lower and higher limits reported previously by Gillespie *et al.* [14].

$E_{\text{c.m.}}$ [keV]	$\omega\gamma_{\text{prev,low}}$ [eV]	$\omega\gamma_{\text{prev,high}}$ [eV]	$\omega\gamma_{\text{pres}}$ [eV]
495.5(6)	$3.0(3) \times 10^{-2}$	$4.7(5) \times 10^{-2}$	$1.37(22) \times 10^{-2}$
471(2)	$3.3(1) \times 10^{-5}$	$7.0(3) \times 10^{-4}$	$9.4(29) \times 10^{-5}$
452(2)	$2.7(3) \times 10^{-3}$	$2.7(3) \times 10^{-3}$	$\leq 3.1 \times 10^{-5}$
431(4)	–	–	$\leq 3.9 \times 10^{-5}$
407(2)	$9.4(12) \times 10^{-4}$	$1.0(1) \times 10^{-3}$	$8.0(19) \times 10^{-4}$
390(2)	$2.4(3) \times 10^{-4}$	$1.5(1) \times 10^{-3}$	$\leq 6.9 \times 10^{-6}$
303(2)	$2.4(2) \times 10^{-8}$	$4.1(8) \times 10^{-6}$	$\leq 7.2 \times 10^{-6}$
272(2)	$8.5(10) \times 10^{-6}$	$8.9(10) \times 10^{-6}$	$1.22(36) \times 10^{-5}$

energies were limited to the determination if a strength existed that could compete with the already measured contributions (495 keV, 272 keV) to the astrophysical reaction rate. The energies probed focused with one exception on the states measured in the work by Gillespie *et al.* [14]. Two of the additional unmeasured potential resonances were expected at 407 and 471 keV. For this work, beam was provided at 426.7 and 492.5 keV/u, respectively, with gas target pressures of 5.89(3) and 6.09(1) Torr.

For the 407 keV resonance, 221(15) recoils were detected after background subtraction. This resonance was only probed for 1.5 h as it became clear that this state's astrophysical reaction rate at peak novae temperatures was below the 272 keV resonance's contribution. With $5.2(3) \times 10^{14}$ ions on target and 41.0(16)% in the chosen charge state of 6^+ , the resonance strength was found to be $8.0(19) \times 10^{-4}$ eV.

For the 471 keV state after background subtraction 30(6) recoils remained. Again, this state's astrophysical significance was seen to be lower than the contribution from both the 495 keV and the 272 keV resonances, so only 4.5 h of data was taken. The chosen recoil charge state of 8^+ was measured to contain 22.3(23)% of the CSD total. After calculating the number of beam ions on target of $1.64(4) \times 10^{15}$ the resonance strength was found to be $9.4(29) \times 10^{-5}$ eV.

For the remaining states probed during this experiment, $E_{\text{c.m.}} = 303, 390, 431, 452$ keV, no positive recoil product detection above background could be recorded. As a result, only upper limits for the resonance strengths were set using the method described by Helene [42]. Again a separator TOF range of 200 ns was used when analyzing the recoil spectra determining the upper limit resonance strengths. These are shown in Table IV together with a summary of all measured strength values. An error budget listing the sources of error considered for the confirmed resonances is given in Table V. All errors contributions are based on experiment or Monte Carlo simulation and combined in quadrature.

D. Astrophysical reaction rate

In order to calculate the astrophysical reaction rate the equation

$$N_A(\sigma v) = N_A \left(\frac{2\pi}{m_0 k T} \right)^{\frac{3}{2}} \hbar^2 e^{-\frac{E_r}{kT}} \omega \gamma \quad (11)$$

TABLE V. Summary of error components in percent (to be applied as a \pm interval on the respective values); added in quadrature and shown as total for the resonances investigated in this work.

Resonance energy [keV]	495.5(6)	471(2)	407(2)	272(2)
Source of error	\pm Error [%]			
BGO efficiency	10.1	17.6	18.1	17.3
Charge state fraction	5.5	10.3	3.9	9.8
Target transmission	1.9	1.8	1.4	3.0
Live time correction	0.9	3.1	0.5	0.9
Separator transmission	0.1	0.1	0.1	0.1
MCP grid transmission	1.2	1.2	1.2	1.2
Hybrid efficiency	0.8	6.2	4.6	0.7
Target pressure	2.6	1.0	1.1	1.0
Target temperature	0.8	0.8	0.8	0.8
Stopping power	10.6	10.1	10.6	8.2
Integrated beam particles	1.9	2.4	5.8	7.8
Recoils detected	0.7	20.0	6.8	18.8
Total	16.2	31.3	23.7	29.8

was used. Here, N_A is Avogadro's number, m_{01} is the reduced mass, $\frac{m_0 m_1}{m_0 + m_1}$, k is the Boltzmann constant, T is the temperature, \hbar is the reduced Planck's constant, E_r (c.m. system) is the resonance energy, and $\omega\gamma$ is the resonance strength. The total rate can be found by adding the individual reaction rates at each temperature. As the calculation is based on directly measured resonances in the relevant energy range, the error of the rate scales with the error in the determined resonance strengths and ranges from approximately $\pm 20\%$ at the higher temperatures to approximately $\pm 30\%$ at the low end of the novae range 0.1–0.48 GK. The uncertainties resulting from this work are smaller than the ones previously presented [14,21], both based on indirect transfer reaction measurements. In Fig. 6, the astrophysical reaction rate for the four confirmed resonance states from this work can be seen.

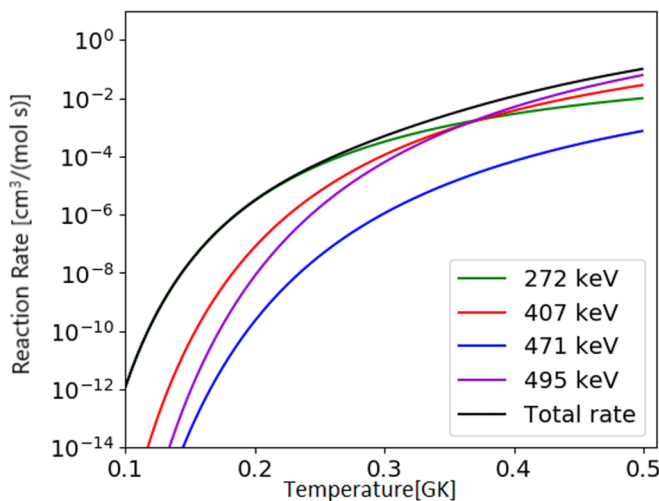


FIG. 6. Astrophysical reaction rate contributions calculated for the four resonances measured in this experiment for the peak nova burning temperature range. Total reaction rate for these four states is shown in black.

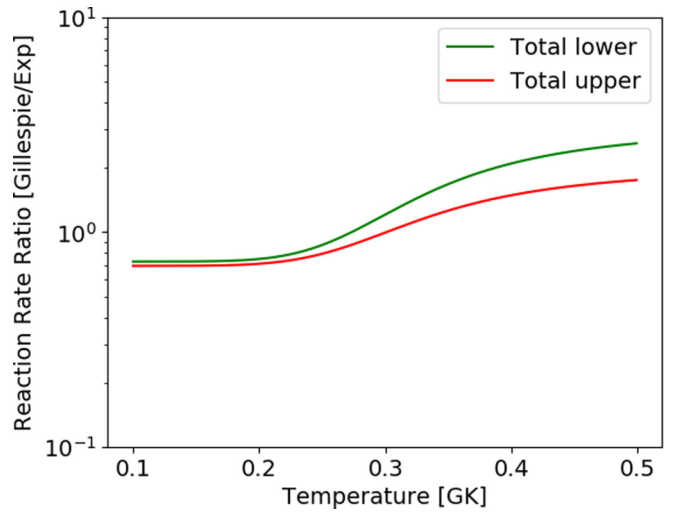


FIG. 7. Total astrophysical reaction rate from the work by Gillespie *et al.* (upper and lower limits) [14] divided by the total rate derived from this work.

The total reaction rate for only these four states can be seen in the solid black. No additional states from the Gillespie [14] or the TUNL [21] measurements were included in the total rate as they either have not been directly confirmed as resonant states or their predicted or measured upper limit strengths result in astrophysical reaction rates that would only slightly alter the total. From the resonance strengths measured in this work, the newly determined 272 keV resonance dominates the astrophysical reaction rate until approximately 0.35 GK when the 407 and 495 keV resonances begin to dominate. It is therefore expected to be of significant importance for the production of ^{35}Cl in nova environments.

VI. SUMMARY AND OUTLOOK

In this work, we have directly measured low energy resonance strengths in the $^{34}\text{S}(p, \gamma)^{35}\text{Cl}$ reaction in inverse kinematics using the DRAGON recoil separator. For the first time the absolute strength of the 495 keV resonant state was measured independently of a reference state, with a result indicating a preferred value of 4.9(5) eV in previously discrepant experiments on the 1177 keV resonance strength. Additionally, three resonances, predicted from indirect experiments, were for the first time directly measured and confirmed to be resonant states. The one at 272 keV dominates the astrophysical reaction rate at peak nova burning temperatures. For several other potential states no recoil reaction products were detected above background and upper limits on their potential resonance strengths were set. If the total astrophysical reaction rate for the states measured in this work is compared to the results of Gillespie *et al.* [14] (see Fig. 7), it can be seen that the total astrophysical reaction rate was underestimated at temperatures below 0.25 GK and overestimated at higher temperatures. However, given that the original strength assignment for the 272 keV resonance was based on a transfer reaction, the experiments agree well.

Our strength value for the previously known resonance at 495 keV should prompt a reevaluation of the strengths of all resonances higher in energy to allow for their inclusion in astrophysical reaction rate calculations for higher temperatures. We would expect that the current uncertainties of the measurement in the temperature range covered would be sufficient for studies of nova nucleosynthesis and their impact on sulfur isotopic ratios in presolar meteoritic grains given the uncertainties in astrophysical modeling and isotope analysis. Should a case be made for further uncertainty reduction, a targeted experiment with emphasis on just the two to three most important resonances could likely achieve another factor 2 smaller errors specifically through event statistics, stopping power determination, and measurements of γ ray branching ratios.

ACKNOWLEDGMENTS

The authors thank the ISAC operations and technical staff at TRIUMF. TRIUMF's core operations are supported via a contribution from the federal government through the National Research Council Canada, and the Government of British Columbia provides building capital funds. DRAGON is supported by funds from the Canadian Natural Sciences and Engineering Research Council (NSERC) Project No. SAPPJ-2019-00039. The Colorado School of Mines group wishes to acknowledge the support of this work through the U.S. Department of Energy (DOE) Office of Science DE-FG02-93ER40789. Further external experimenters were supported in part by Canadian NSERC (McMaster) and U.S. National Science Foundation [NSF: PHY-1565546 (MSU), PHY-1401343 + PHY-1419765 (ND)].

-
- [1] J. D'Auria *et al.*, The $^{21}\text{Na}(p, \gamma)^{22}\text{Mg}$ reaction from $E_{\text{c.m.}} = 200$ to 1103 keV in novae and x-ray bursts, *Phys. Rev. C* **69**, 065803 (2004).
- [2] J. José and M. Hernanz, Nucleosynthesis in classical novae: CO versus ONe white dwarfs, *Astrophys. J.* **494**, 680 (1998).
- [3] C. Iliadis, *Nuclear Physics of the Stars* (Weinheim, Germany, 2015).
- [4] C. E. Rolfs and W. S. Rodney, *Cauldrons in the Cosmos: Nuclear Astrophysics* (University of Chicago Press, Chicago, 1988).
- [5] A. Kovetz and D. Prialnik, The composition of nova ejecta from multicycle evolution models, *Astrophys. J.* **477**, 356 (1997).
- [6] B. Schaefer, Comprehensive photometric histories of all known galactic recurrent novae, *Astrophys. J. Suppl. Ser.* **187**, 275 (2010).
- [7] A. Shafter, The galactic rate revisited, *Astrophys. J.* **834**, 196 (2017).
- [8] S. Amari, X. Gao, L. R. Nittler, E. Zinner, J. José, M. Hernanz, and R. S. Lewis, Presolar grains from novae, *Astrophys. J.* **551**, 1065 (2001).
- [9] L. Nittler and F. Ciesla, Astrophysics with extraterrestrial materials, *Annu. Rev. Astron. Astrophys.* **54**, 53 (2016).
- [10] P. Hoppe, J. Leitner, E. Gröner, K. K. Marhas, B. S. Meyer, and S. Amari, NanoSIMS studies of small presolar SiC grains: New insight into supernova nucleosynthesis, chemistry, and dust formation, *Astrophys. J.* **719**, 1370 (2010).
- [11] J. José, M. Hernanz, S. Amari, K. Lodders, and E. Zinner, The imprint of nova nucleosynthesis in presolar grains, *Astrophys. J.* **612**, 414 (2004).
- [12] P. Hoppe, W. Fujiya, and E. Zinner, Sulfur molecule chemistry in supernova ejecta recorded by silicon carbide stardust, *Astrophys. J. Lett.* **745**, L26 (2012).
- [13] A. Parikh, K. Wimmer, T. Faestermann, J. José, R. Hertenberger, H.-F. Wirth, C. Hinke, R. Kruecken, D. Seiler, K. Steiger, and K. Straub, Isotopic $^{32}\text{S}/^{33}\text{S}$ ratio as a diagnostic of presolar grains from novae, *Phys. Lett. B* **737**, 314 (2014).
- [14] S. A. Gillespie, A. Parikh, C. J. Barton, T. Faestermann, J. José, R. Hertenberger, H.-F. Wirth, N. de Séréville, J. E. Riley, and M. Williams, First measurement of the $^{34}\text{S}(p, \gamma)^{35}\text{Cl}$ reaction rate through indirect methods for presolar nova grains, *Phys. Rev. C* **96**, 025801 (2017).
- [15] C. Iliadis, A. Champagne, J. José, S. Starrfield, and P. Tupper, The effects of thermonuclear reaction rate variations on nova nucleosynthesis: A sensitivity study, *Astrophys. J. Suppl. Ser.* **142**, 105 (2002).
- [16] O. P. Van Pruissen, G. J. L. Nooren, and C. Van Der Leun, Primary gamma-ray transitions of mixed E1 + M2 character, *Nucl. Phys. A* **480**, 77 (1988).
- [17] N. Hazewindus, W. Lourens, A. Scheepmaker, and A. H. Wapstra, Gamma ray transitions in ^{35}Cl , *Physica* **29**, 681 (1963).
- [18] G. Engelbertink and P. Endt, Measurements of (p, γ) resonance strengths in the s-d shell, *Nucl. Phys.* **88**, 12 (1966).
- [19] M. Aléonard, C. Boursiquot, P. Hubert, and P. Mennrath, Strengths of (p, γ) resonances in ^{33}Cl , ^{35}Cl , and ^{28}Si , *Phys. Lett. B* **49**, 40 (1974).
- [20] M. Meyer, I. Venter, W. F. Coetzee, and D. Reitmann, Energy levels of ^{35}Cl , *Nucl. Phys. A* **264**, 13 (1976).
- [21] K. Setoodehnia, J. H. Kelley, C. Marshall, F. Portillo Chaves, and R. Longland, Experimental study of ^{35}Cl excited states via $^{32}\text{S}(\alpha, p)$, *Phys. Rev. C* **99**, 055812 (2019).
- [22] A. Graue, L. H. Herland, J. R. Lien, G. E. Sandvik, E. R. Cosman, and W. H. Moore, A study of the ^{35}Cl levels by means of the $^{34}\text{S}(\text{He}, d)^{35}\text{Cl}$ reaction, *Nucl. Phys. A* **136**, 577 (1969).
- [23] M. Soltani-Farshi, J. D. Meyer, P. Misaelides, and K. Bethge, Cross section of the $^{32}\text{S}(\alpha, p)^{35}\text{Cl}$ nuclear reaction for sulphur determination, *Nucl. Instrum. Methods Phys. Res. B* **113**, 399 (1996).
- [24] R. Laxdal, Acceleration of radioactive ions, *Nucl. Instrum. Methods Phys. Res. B* **204**, 400 (2003).
- [25] K. Jayamanna *et al.*, A multicharge ion source (supernanogan) for the OLIS facility at ISAC/TRIUMF, *Rev. Sci. Instrum.* **81**, 02A331 (2010).
- [26] D. Hutcheon *et al.*, The DRAGON facility for nuclear astrophysics at TRIUMF-ISAC, *Nucl. Phys. A* **718**, 515 (2003).
- [27] D. Hutcheon *et al.*, The DRAGON facility for nuclear astrophysics at TRIUMF-ISAC: Design, construction and operation, *Nucl. Instrum. Methods Phys. Res. A* **498**, 190 (2003).
- [28] C. Vockenhuber *et al.*, Improvements of the DRAGON recoil separator at ISAC, *Nucl. Instrum. Methods Phys. Res. B* **266**, 4167 (2008).

- [29] U. Greife *et al.*, Energy loss around the stopping power maximum of Ne, Mg, and Na ions in hydrogen gas, *Nucl. Instrum. Methods Phys. Res. B* **217**, 1 (2003).
- [30] D. Connolly, Radiative alpha capture on ^{34}S at astrophysically relevant energies and design of a scattering chamber for high precision elastic scattering measurements for the Dragon experiment, Ph.D. thesis, Colorado School of Mines, 2015.
- [31] D. Gigliotti, Efficiency calibration measurement and GEANT simulation of the DRAGON BGO gamma ray array at TRIUMF, Master's thesis, University of Northern British Columbia, 2000.
- [32] D. Gigliotti, J. G. Rogers, and A. H. Hussein, Calibration and simulation of a gamma array for DRAGON at ISAC, *Nucl. Instrum. Methods Phys. Res. B* **204**, 671 (2003).
- [33] S. Engel *et al.*, Commissioning the DRAGON facility at ISAC, *Nucl. Instrum. Methods Phys. Res. A* **533**, 491 (2005).
- [34] D. Hutcheon *et al.*, Background suppression by the DRAGON radiative capture facility at TRIUMF-ISAC, *Nucl. Instrum. Methods Phys. Res. B* **266**, 4171 (2008).
- [35] J. Slater, GEANT Simulation of DRAGON and the $^{12}\text{C}(^{12}\text{C}, \gamma)^{24}\text{Mg}$ reaction, B.S. thesis, University of Waterloo, 2004.
- [36] P. Endt, Energy levels of A=21-44 nuclei (VII), *Nucl. Phys. A* **521**, 1 (1990).
- [37] W. Liu, Charge state studies of heavy ions passing through matter, Master's thesis, Simon Fraser University, 2001.
- [38] W. Liu *et al.*, Charge state studies of low energy heavy ions passing through hydrogen and helium gas, *Nucl. Instrum. Methods Phys. Res. A* **496**, 198 (2003).
- [39] J. F. Ziegler, M. D. Ziegler, and J. P. Biersack, SRIM - the stopping range of ions in matter (2010), *Nucl. Instrum. Methods Phys. Res. B* **268**, 1818 (2010).
- [40] G. Schiwietz and P. L. Grande, Improved charge-state formulas, *Nucl. Instrum. Methods Phys. Res. B* **177**, 125 (2001).
- [41] M. Lovely, Proton capture on ^{34}S in the astrophysical energy regime, Ph.D. thesis, Colorado School of Mines, 2020.
- [42] O. Helene, Determination of the upper limit of a peak area, *Nucl. Instrum. Methods Phys. Res. A* **300**, 132 (1991).